

ELK3-CXCL16 axis determines natural killer cell cytotoxicity via the chemotactic activity of CXCL16 in triple negative breast cancer

Hae-Yun Jung^{a,†}, Dae-Keum Lee^{a,†}, Minwook Lee^a, Seung Hee Choia, Joo Dong Park^a, Eun-Su Ko^a, Jongwon Lee^b, Kyung-Soon Park^a, and Hae-Yun Jung^{a,c}

^aDepartment of Biomedical Science, College of Life Science, CHA University, Seongnam-si, Gyeonggi-do, Republic of Korea; ^bBrain Korea 21 Plus Project for Biomedical Science, Korea University College of Medicine, Seoul, Republic of Korea; ^cDivision of Radiation Biomedical Research, Korea Institute of Radiological and Medical Sciences, Seoul, Republic of Korea

ABSTRACT

Triple-negative breast cancer (TNBC) is the most challenging subtype of breast cancer because of its aggressive behavior and the limited therapeutic strategies available. In the last decade, immunotherapy has become a promising treatment to prolong survival in advanced solid cancers including TNBC. However, the efficacy of immunotherapy in solid cancers remains limited because solid tumors contain few tumor-infiltrating lymphocytes. Here, we show that targeting an ETS transcription factor ELK3 (ELK3) recruits immune cells including natural killer (NK) cells into tumors via the chemotactic activity of chemokine. ELK3 depletion increases CXCL16 expression level and promotes NK cell cytotoxicity through CXCL16-mediated NK cell recruitment in TNBC. *In silico* analysis showed that *ELK3* is negatively correlated with *CXCL16* expression in breast cancer patient samples. Low expression of *ELK3* and high expression of *CXCL16* were associated with a better prognosis. Low expression of *ELK3* and high expression of *CXCL16* were associated with increased expression of NK cell-related genes. Our findings demonstrate that the ELK3-CXCL16 axis modulates NK cell recruitment to increase NK cell cytotoxicity, suggesting that targeting the *ELK3* gene could be an adjuvant strategy for increasing the efficacy of immunotherapy in TNBC.

ARTICLE HISTORY

Received 19 October 2022
Revised 10 March 2023
Accepted 10 March 2023

KEYWORDS

CXCL16; ELK3; immunosuppressive tumor microenvironment; NK cell cytotoxicity; NK cell recruitment; triple-negative breast cancer

I Introduction

Current immunotherapy is an alternative strategy for the treatment of refractory solid cancers after traditional cancer treatments.^{1,2} Immunotherapies, including T cell immunotherapy, have improved the survival rate of advanced cancer patients.^{3–6} However, T cell immunotherapy faces several challenges for broad clinical application, such as the lack of tumor-infiltrating lymphocytes, difficulty with genetic engineering, high toxicity, and disease progression.^{7,8} Due to the limitations of T cell immunotherapy, a new approach to cellular immunotherapy is necessary in advanced solid tumors.

Natural killer (NK) cells are key members of the innate immune system that activate the adaptive immune system by releasing cytokines and chemokines.^{9,10} NK cells also play a critical role in immunosurveillance to control cancer progression.^{11–13} NK cells are activated by the recognition of activating and inhibitory receptors-ligands, as well as by soluble factors such as cytokines in the tumor microenvironment (TME).^{14,15} However, in the immunosuppressive TME, NK cells lose cell cytotoxicity, resulting in dysfunctional NK cells that trigger cancer progression.^{16,17} Understanding the molecular mechanisms underlying the regulation of NK cell activation may facilitate the development of NK cell therapy as an alternative immune cell therapy.

Although biopsies from cancer patients show low levels of infiltrating NK cells in tumor tissues, NK cell infiltrates are associated with a good prognosis in several solid tumors including melanoma and gastric cancer.^{18–20} Therefore, NK cell recruitment to the tumor is an essential step to improve the anticancer effect of NK cells. Chemokines can promote a change in the TME from immune-suppressive to immune-sensitive.^{21,22} However, the molecular mechanisms underlying NK cell recruitment to solid tumors remain unclear.

ELK3, an ETS transcription factor, functions as an oncogene in various cancers including TNBC.^{23–27} ELK3 contributes to cancer metastasis by regulating cell migration-related genes.^{28,29} ELK3 is involved in chemokine regulation that VEGF mediates lymphatic endothelial cell migration in lymphangiogenesis and also regulates macrophage recruitment in the immune response.^{30–33} However, the role of ELK3 in anticancer immune responses is still not clear.

Here, we report that targeting ELK3 might be a promising strategy for boosting the efficacy of immunotherapy in TNBC. ELK3 depletion increased the sensitivity to NK cell cytotoxicity by inhibiting the inhibitory ligand of tumor cells and the inhibitory receptor of NK cells. Also, ELK3 depletion significantly induced a chemokine such as CXCL16. *In vitro* and *in vivo* studies showed that CXCL16 promoted NK cell recruitment to target tumor cells. CXCL16-induced NK cell

CONTACT Kyung-Soon Park ✉ kspark@cha.ac.kr; Hae-Yun Jung ✉ hyjung@kirams.re.kr  Division of Radiation Biomedical Research, Korea Institute of Radiological and Medical Sciences, Seoul, Republic of Korea

†These authors contributed equally to this work.

 Supplemental data for this article can be accessed online at <https://doi.org/10.1080/2162402X.2023.2190671>

© 2023 The Author(s). Published with license by Taylor & Francis Group, LLC.

This is an Open Access article distributed under the terms of the Creative Commons Attribution-NonCommercial License (<http://creativecommons.org/licenses/by-nc/4.0/>), which permits unrestricted non-commercial use, distribution, and reproduction in any medium, provided the original work is properly cited. The terms on which this article has been published allow the posting of the Accepted Manuscript in a repository by the author(s) or with their consent.

infiltration is important for enhancing NK cell cytotoxicity. *In silico* analysis showed a negative correlation between the *ELK3* and *CXCL16* genes in human breast cancer patients and in TNBC cell lines. Low expression of *ELK3* and high expression of *CXCL16* were associated with a good prognosis and upregulation of NK cell-related genes in human breast cancer patient samples. We demonstrated that the *ELK3*-*CXCL16* axis mediates NK cell recruitment to improve NK cell cytotoxicity in TNBC.

Materials and methods

Cell cultures and reagents

The human NK cell line NK92MI was purchased from the American Type Culture Collection (ATCC). NK92MI cells were cultured in Minimum Essential Medium Alpha (Gibco, 12451056, Grand Island, NY, USA) supplemented with 2 mM L-glutamine (Gibco, 25030-081), 0.2 mM inositol (Sigma, I7508, St. Louis, MO, USA), 0.1 mM 2-mercaptoethanol (Gibco, 21985-023), 0.02 mM folic acid (Sigma, F5758), 12.5% fetal bovine serum, and 1% penicillin-streptomycin (Gibco). The human breast cancer cell line MDA-MB231 was cultured in Dulbecco's modified Eagle's medium (DMEM) (Gibco) supplemented with 10% fetal bovine serum (Gibco) and 1% penicillin-streptomycin (Gibco). The human breast cancer cell line Hs578T was cultured in DMEM (Gibco) supplemented with 10% fetal bovine serum (Gibco), 1% penicillin-streptomycin (Gibco), and 0.01 mg/ml insulin (Sigma, I9278). Human primary NK cells were purified from peripheral blood mononuclear cells (PBMC), as described previously.³⁴ Primary NK cells were cultured in Advanced Roswell Park Memorial Institute 1640 medium with non-essential amino acids (Gibco) supplemented with 10% fetal bovine serum, 1% penicillin-streptomycin, 4 mM GlutaMAX-I Supplement (Gibco), 10 ng/mL human interleukin-2 (PeproTech), and 5 ng/mL interleukin-15 (PeproTech) for 14 days. All cells were incubated at 37°C and 5% CO₂. To generate stable *ELK3*-knockdown cells, shRNA lentiviruses (human *ELK3*, RHS4531-EG2004, Dharmacon Inc., Lafayette, CO, USA) were transduced into target cells with 10 µg/ml protamine sulfate. pLVX-*CXCL16* was generated by cDNA synthesis. The protein coding region of the *CXCL16* gene was ligated into the pLVX vector. To generate stable *CXCL16* overexpressing cells, pLVX-*CXCL16* and pRRL-GFP vectors were transduced into target cells with 10 µg/ml protamine sulfate. The infected cells were selected with 2 µg/ml puromycin. To generate transient gene-knockdown cells, 50 nM siRNA (human *CXCL16* #1 and human *CXCL16* #2, siRNA ID: 58,191-1 and 58191-2; Bioneer, Daejeon, Chungnam, Republic of Korea) was transfected into target cells using Lipofectamine 2000. Recombinant human *CXCL16* protein was purchased from PEPROTECH (300-55, Cranbury, NJ, USA).

Real-time qPCR

RNA was extracted from cells using the Trizol reagent (Invitrogen, Carlsbad, CA, USA). cDNA synthesis was performed using SuperScript™ II Reverse Transcriptase

(Invitrogen), and qPCR was performed using TOPreal™ qPCR 2× PreMIX (Enzynomics, Daejeon, Chungnam, Republic of Korea). The primers used for this study are listed in Supplemental Table 1. Expression values were generated using $\Delta\Delta C_t$ values normalized to GAPDH.³⁵ The experiments were performed in triplicate, both biological and technical, using the CFX Connect (Bio-Rad, Hercules, CA, USA) real-time PCR detection system. For each comparison, unpaired two-tailed Student's t-tests were performed to determine the statistical significance.

Immunoblot analysis

Cells were lysed with Cell Lysis Buffer (Cell Signaling Technology, Inc. Danvers, MA, USA). Total proteins were separated by sodium dodecyl sulfate-polyacrylamide gel electrophoresis (SDS-PAGE) and transferred to poly(vinylidene fluoride) PVDF membranes (Bio-Rad). The membranes were blocked with 5% nonfat milk and then probed overnight at 4°C with anti-*ELK3* (Novus Biologicals, NBP2-01264), anti-*CXCL16* (Santa Cruz Biotechnology, sc-376395), and anti-GAPDH (Santa Cruz Biotechnology, sc-166574, Dallas, Texas, USA) antibodies, followed by washing with TBS-T. After washing, the membranes were incubated for 1 h at RT with a secondary antibody (anti-mouse, GeneTex, GTX213111-01). Immunoreactivity was detected using an ECL kit (Thermo Scientific, Rochester, NY, USA) and ImageQuant Las 4000 (GE Healthcare, Chicago, IL, USA).

3D cell cultures and immunostaining

Cells were seeded on Matrigel (Growth Factor Reduced Matrigel, BD Biosciences, Franklin Lakes, NJ, USA) using 2% Matrigel DMEM media supplemented with 10% fetal bovine serum and penicillin/streptomycin. Immunostaining with cell-based organoids was performed following a previously published protocol.³⁶ Primary antibodies used were anti-E-cadherin (BD Bioscience, 610181) and anti-F-actin (Thermo Fisher, A12381). Images were acquired using a Zeiss LSM 510 microscope and analyzed with ImageJ software.

NK cell cytotoxicity in 3D cell cultures

NK cell-mediated apoptosis was analyzed using CellEvent® Caspase-3/7 green detection reagent (Invitrogen, C10423). Briefly, the cells were cultured in a 3D culture system for 4 days and cocultured with FarRed (Invitrogen, C34564)-labeled NK92MI cells for 4 h. Apoptotic cells were stained with Caspase-3/7 green reagent following the manufacturer's protocol and visualized under the microscope. Images were acquired using a Zeiss LSM510 microscope and analyzed with ImageJ software.

In vitro NK cell cytotoxicity assay

Cancer cells were cocultured with CFSE (Invitrogen, C34554)-labeled NK92MI cells for 4 h and then stained with 7AAD (Invitrogen, A1310) to analyze NK cell-mediated cell death. CFSE-7AAD-positive cells were counted as target cell death

using a CytoFLEX flow cytometer (Beckman Coulter, Brea, CA, USA).

Chemotaxis assay

NK cell mobility was analyzed using a Transwell insert (Corning, 3422, Corning, NY, USA). Cells (1×10^5) were seeded in 24-well plates and cultured for 24 h. A total of 1×10^5 CFSE or FarRed-labeled NK92MI cells were seeded in the Transwell insert in serum-free medium, and the insert was loaded into 24-well plates. After 6 h or 24 h, migrated NK92MI cells were visualized under a microscope. Images were acquired using a Zeiss LSM510 microscope or EVOS M5000 and analyzed with ImageJ software.

Secreted proteins analysis

Cells were cultured for 24–48 h, and the conditioned medium was harvested from the culture. The analysis of secreted proteins in conditioned medium was performed using the proteome profiler human angiogenesis array kit (R&D system, Minneapolis, MN, USA) according to the manufacturer's protocol.

Flow cytometry

Cells were washed with fluorescence-associated cell sorting (FACS) buffer (BD Bioscience, 554656) and blocked with Fc blocker (BD Bioscience, 564220) for 30 min at room temperature. Cells were stained with fluorescence-conjugated primary antibodies for 30 min on ice, washed twice with FACS buffer, and fixed with 2% PFA for 15 min. For non-conjugated primary antibodies, the cells were incubated with primary antibodies overnight at 4°C and incubated with secondary antibodies for 60 min at room temperature. Samples were analyzed using a CytoFLEX flow cytometer (Beckman Coulter). Primary antibodies used were as follows: anti-CD107a (BD Biosciences, 560664), anti-IFN γ (BioLegend, 554701, San Diego, CA, USA), anti-NKG2A (BioLegend, 375103), anti-CD96 (BioLegend, 562379), anti-NKG2D (BD Biosciences, 557940), anti-CD16 (Invitrogen, MHCD1604), anti-ULBP-1 (R&D Systems, MAB1380), anti-ULBP-2/5/6 (R&D Systems, MAB1289), anti-ULBP-3 (R&D Systems, MAB1517), anti-MIC-A/B (Invitrogen, 12-5788-42), anti-HLA-ABC (BD Biosciences, 557349), anti-HAL-E (Invitrogen, 12-9953-41), anti-HLA-G (Invitrogen, 12-9957-41), and CXCR6 (BioLegend, 151103). For CD107a and IFN γ staining, cells were treated with brefeldin A (BioLegend, 420601) for 5 h before incubation with the primary antibody.

Microarray analysis

Microarray data of MDA-MB231 cells were downloaded from the GEO database (GSE83325).³⁷ Affymetrix expression microarray analysis of the Hs578T cell line was performed by BioCore. Briefly, the library was constructed using the standard Affymetrix protocol. Labeled DNA was hybridized to the Affymetrix GeneChip Array (Affymetrix, Santa Clara, CA, USA) and scanned on a GCS3000 scanner (Affymetrix). Data

processing and analysis were performed using Affymetrix GeneChip Command Console Software (Affymetrix). Genes with fold change >1.50 and $p < 0.05$ were first selected. Gene lists were sorted using the KEGG mapper tool (<https://www.genome.jp/kegg/mapper/>). Gene clustering and heatmaps were analyzed using the MeV tool (version 4.9.0). The Hs578T microarray data are deposited in the Gene Expression Omnibus data repository under the code GSE208584. Gene expression data from breast cancer cell lines were downloaded from the Cancer Dependency Map (DepMap). Gene expression data were obtained from 24 breast cancer cell lines.

TCGA analysis of breast cancer patients

Gene expression and survival analyses of 421 breast cancer patient samples from TCGA databases were performed on the cBioportal website (<https://www.cbioportal.org/>). For large-scale survival analysis, RNA-seq data from TCGA were retrieved using R/Bioconductor package TCGAbiolinks³⁸ version 2.18.0. Breast cancer (TCGA-BRCA) normalized expression data of 1215 cases, including 1095 primary tumors, 7 metastatic tumors, and 113 normal tissues aligned to the hg19 reference genome, were downloaded using the GDC download function from NCI's Genomic Data Commons (GDC) <https://portal.gdc.cancer.gov/>. Survival analysis was performed using clinical metadata from TCGA depending on whether the expression of *ELK3* and *CXCL16* in each sample was higher (high expression) or lower (low expression) than the median. TCGA analyze_survival function was used, and the significance level was set at 0.05 for group comparisons in the survival analysis. A p-value <0.05 was considered significant. NK cell-related genes were selected from the published data.³⁹ Gene correlations of 1,085 breast cancer patient samples from TCGA database were analyzed using the Gene Expression Profiling Interactive Analysis 2 (GEPiA2) website (<http://gepia2.cancer-pku.cn>). The correlation coefficient was calculated using Pearson's Correlation, and a p-value <0.05 was considered to indicate a statistically significant difference.

Mouse experiments

To establish the experimental metastasis model, 2×10^6 MDA-MB231 cells expressing GFP-luciferase were intravenously injected into 7-week-old female BALB/c nude mice. After 4 weeks, mice were treated with 1×10^7 FarRed-labeled NK92MI cells by intravenous (IV) injection three times within a week. Mice were sacrificed to harvest lung tissue. To establish an MDA-MB231 orthotopic mouse model, 5×10^6 cells expressing GFP-luciferase were injected into the mammary gland of 7-week-old female NOD-SCID gamma (NSG) mice. When tumors were formed, mice were treated with 1×10^7 FarRed-labeled NK92MI cells by intravenous (IV) injection every other day. Tumor size was monitored twice a week. Mice were sacrificed to harvest tumor and lung tissues. To analyze the NK cell recruitment, harvested tissues were digested with Accumax (Sigma-Aldrich, A70890), and tumor cells and NK cells were isolated by removing red blood cells using RBC lysis buffer (Biolegend, 42030). The portion of GFP-labeled tumor cells and FarRed-labeled NK92MI cells was analyzed using

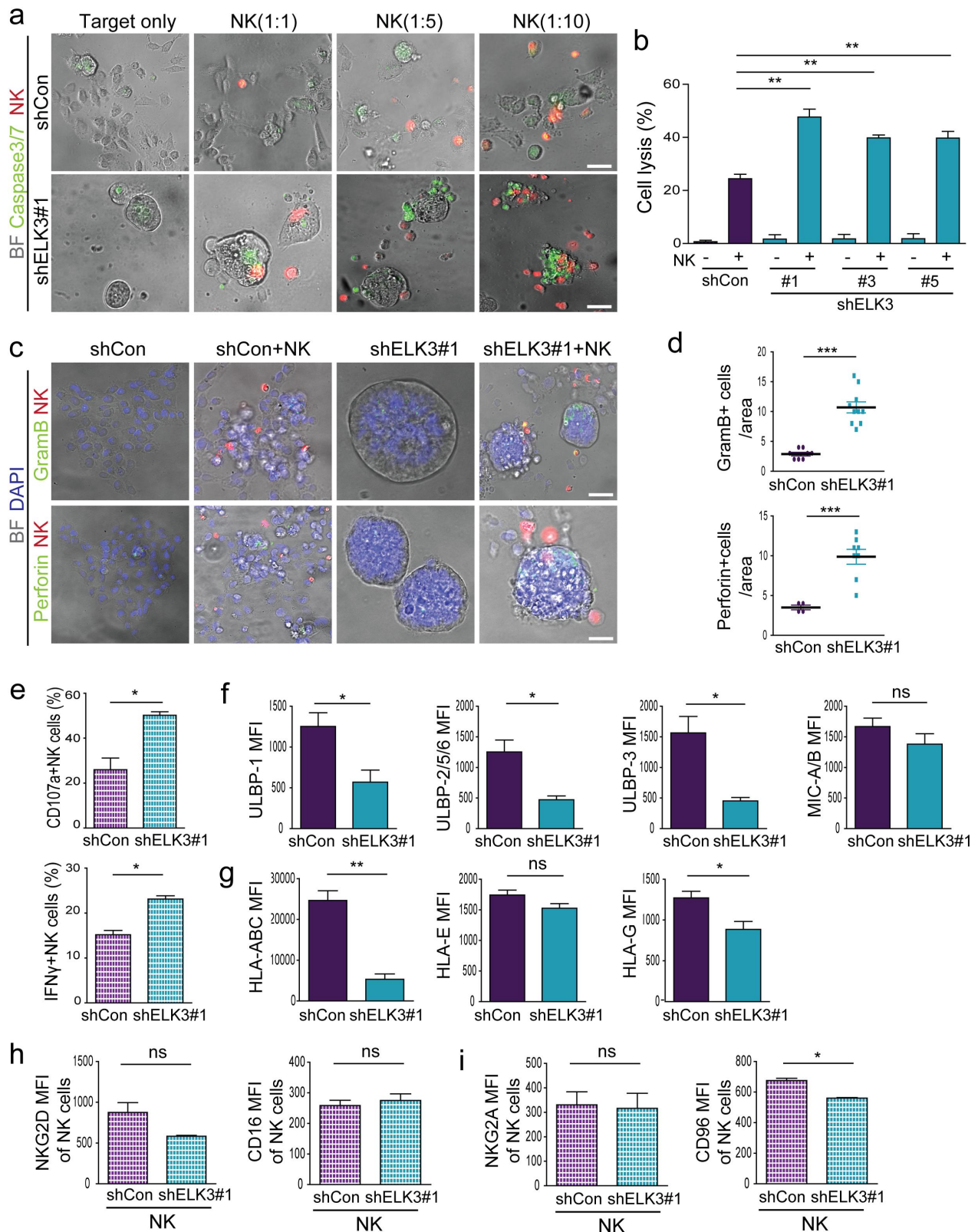


Figure 1. ELK3 depletion increases NK cell cytotoxicity regardless of E-cadherin expression. (a) Immunofluorescence images of caspase 3/7 activity (green) in MDA-MB231 organoids expressing shCon and shELK3#1 after 4 h of coculture with FarRed-labeled NK92MI cells. The E:T ratio is presented as 1:1, 1:5, and 1:10. Scale bar, 100 μ m. (b) Rate of target cell death in MDA-MB231 cells expressing shCon, shELK3#1, shELK3#3, and shELK3#5 after 4 h of coculture with CFSE-labeled NK92MI cells. The E:T ratio is 1:10. Error bars represent standard deviation; ** $p < 0.01$ (one-way ANOVA). (c) Immunofluorescence images of perforin and granzymeB in MDA-MB231 organoids expressing shCon and shELK3#1 after 4 h of coculture with FarRed-labeled NK92MI cells. The E:T ratio is 1:10. Scale bar, 50 μ m. (d) The quantified graft of granzymeB and perforin protein. Error bars represent standard deviation; *** $p < 0.001$ (unpaired two-tailed Student's t-test). (e) The percentage of CD107a-positive and IFN- γ -positive NK92MI cells in MDA-MB231 cells expressing shCon and shELK3#1 after 4 h of coculture with NK92MI cells. Error bars represent standard deviation; * $p < 0.05$ (unpaired two-tailed Student's t-test). (f-g) Quantitative analysis of indicated ligands in MDA-MB231 cells expressing shCon and shELK3#1. Error bars represent standard deviation; * $p < 0.05$, NS is non-significant (unpaired two-tailed Student's t-test). (h-i) Quantitative analysis of indicated receptors in MDA-MB231 cells expressing shCon and shELK3#1. Error bars represent standard deviation; * $p < 0.05$, NS is non-significant (unpaired two-tailed Student's t-test).

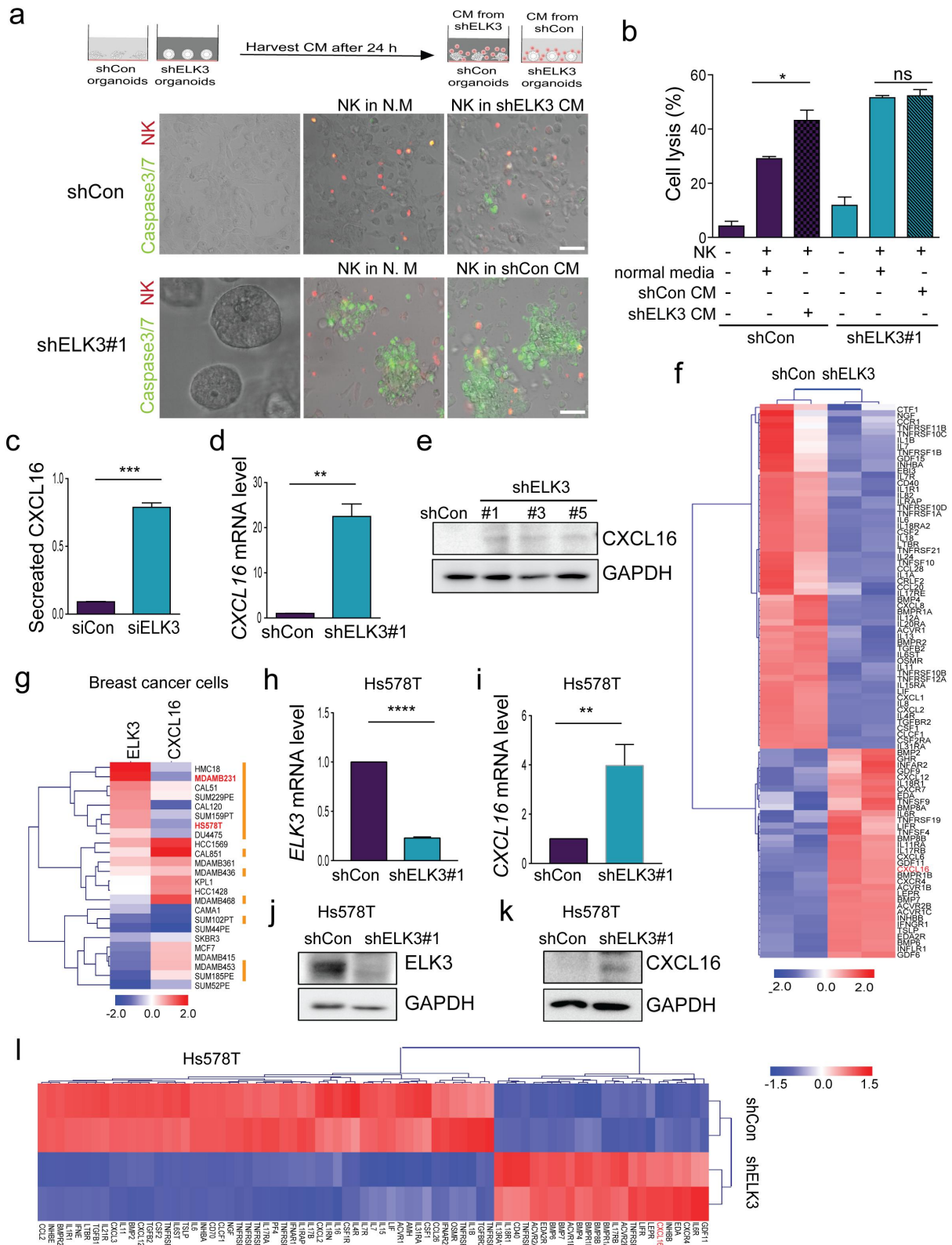


Figure 2. ELK3 depletion increases CXCL16 expression in TNBC cells. (a) Experimental scheme for assessing NK cell cytotoxicity using conditioned medium (CM) from MDA-MB231 organoids expressing shCon and shELK3#1. CM from MDA-MB231 organoids was applied to MDA-MB231 organoids expressing shELK3#1 for NK92MI cell coculture; conversely, CM from MDA-MB231 organoids expressing shELK3#1 was applied to MDA-MB231 organoids expressing shCon for NK92MI cell coculture. N. M. represents normal media. Immunofluorescence images of caspase 3/7 activity (green) in MDA-MB231 organoids expressing shCon and shELK3#1 after 4 h of coculture with FarRed-labeled NK92MI cells under the indicated conditions. The E:T ratio is 1:10. Scale bar, 100 μ m. (b) Rate of target cell death in MDA-MB231 cells expressing shCon and shELK3#1 after 4 h of coculture with CFSE-labeled NK92MI cells under the indicated conditions. The E:T ratio is 1:10. Error bars represent standard deviation; * $p < 0.05$ (unpaired two-tailed Student's *t*-test). NS is non-significant. (c) Quantification of secreted CXCL16 protein in MDA-MB231 cells transfected with siCon and siELK3. Error bars represent standard deviation; *** $p < 0.001$ (unpaired two-tailed Student's *t*-test). (d) Quantitative analysis of CXCL16 mRNA levels in MDA-MB231 cells expressing shCon and shELK3#1. Error bars represent standard deviation; ** $p < 0.01$ (unpaired two-tailed Student's *t*-test). (e) Immunoblot analysis of the CXCL16 protein in MDA-MB231 cells expressing shCon, shELK3#1, shELK3#3, and shELK3#5. GAPDH was used as the loading control. (f) Heatmap analysis of immune-related genes in MDA-MB231 cells expressing shCon and shELK3#1. (g) Correlation analysis of ELK3 and CXCL16 in various breast cancer cells. Orange line indicates TNBC

a CytoFLEX flow cytometer (Beckman Coulter). To visualize recruited NK cells in the lung, frozen lung tissue was observed for the presence of GFP-labeled tumor cells and FarRed-labeled NK92MI cells under a Zeiss LSM510 microscope. All animal care and experiments were performed in accordance with the animal protocol approved by Institutional Animal Care and Use Committee of CHA University (IACUC210067, CHA University, Seongnam, Gyeonggi, Republic of Korea).

Statistical analysis

Statistical analysis was performed using GraphPad Prism software. P-values were derived from unpaired two-tailed Student's t-tests and two-way ANOVA for multiple comparisons. Error bars indicate standard deviation (SD). Statistical significance was considered as $p < 0.05$. Significance levels were reported as * $p < 0.05$, ** $p < 0.01$, *** $p < 0.001$, and **** $p < 0.0001$. All data were derived from at least three independent biological experiments.

Results

ELK3 depletion enhances NK cell cytotoxicity in the E-cadherin independent manner

A previous report suggested that ELK3 negatively regulates E-cadherin to promote epithelial–mesenchymal transition²⁶. ELK3 depletion in MDA-MB231 organoids induced epithelial characteristics including increased E-cadherin expression and decreased F-actin expression (Supplemental Figure 1a-c). Because E-cadherin is a ligand of the inhibitory receptor KLRG-1 in NK cells,^{40,41} we investigated whether the effect of ELK3 depletion on the immune response of NK cells in TNBC. Unexpectedly, ELK3 depletion significantly increased apoptosis and cell death compared with the control (Figure 1a-b). Consistent with NK cell cytotoxicity, granzyme B, perforin, CD107a, and IFN γ , which are indicators of activated NK cells, were accumulated in ELK3-depleted MDA-MB231 organoids and cells (Figure 1c-e). We analyzed the activating and inhibitory receptors/ligands of NK cells in control and ELK3-depleted MDA-MB231 cells. Activating and inhibitory ligands on cancer cells were significantly decreased in ELK3-depleted MDA-MB231 cells (Figure 1f-g). Additionally, activating and inhibitory receptors of NK cells did not differ between control and ELK3-depleted cells except for an inhibitory receptor of CD96 (Figure 1h-i). These results indicate that ELK3 depletion promotes NK cell-mediated cell death regardless of E-cadherin expression.

ELK3 depletion increases CXCL16 expression in TNBC cell lines

Given that the immune response of NK cells is associated with chemokines,^{42,43} we examined whether secreted factors control NK cell cytotoxicity in ELK3-depleted MBA-MB231 cells. Conditioned medium (CM) from control and ELK3-depleted organoids cultures was harvested and inversely applied to control and ELK3-depleted organoids during NK cell coculture. Interestingly, the CM from ELK3-depleted organoids increased NK cell cytotoxicity in control MBA-MB231 organoids (Figure 2a-b), suggesting that the CM from ELK3-depleted MDA-MB231 cells contains secreted factors that increase NK cell cytotoxicity. To address this, we analyzed secreted proteins in the CM from control and ELK3-depleted cells using an immunoassay. Indeed, CXCL16 protein remarkably secreted in the media from ELK3-depleted MDA-MB231 cells (Figure 2c). The mRNA and protein levels of CXCL16 were also increased in ELK3-depleted MDA-MB231 cells (Figure 2d-e). Microarray analysis confirmed that CXCL16 levels were higher in ELK3-depleted MDA-MB231 cells than in control cells (Figure 2f). To extend this finding, we performed *in silico* analysis using various breast cancer cell lines. Most TNBC cell lines showed high expression of *ELK3* and low expression of *CXCL16* (Figure 2g, orange line). ELK3-depleted Hs578T cells also showed induction of *CXCL16* mRNA and protein levels (Figure 2h-k). Microarray analysis confirmed that *CXCL16* levels were higher in ELK3-depleted Hs578T cells than in control cells (Figure 2l). These data suggest that ELK3 depletion increases *CXCL16* protein levels in TNBC cell lines.

CXCL16 contributes to NK cell cytotoxicity through the recruitment of NK cells

To investigate the relation between *CXCL16* induction and increased NK cell cytotoxicity, we examined the effects of *CXCL16* on NK cell-mediated cell death. MDA-MB231 organoids with *CXCL16* recombinant protein treatment during NK cell coculture showed increased NK cell cytotoxicity (Figure 3). We investigated whether *CXCL16* increased NK cell recruitment for enhancing NK cell cytotoxicity because NK cells expressed CXCR6 which was a counterpart of *CXCL16* (Supplemental Figure 2a-b). To examine the effect of *CXCL16* on the migration of NK cells using an *in vitro* Transwell assay, the recombinant *CXCL16* protein induced the migration of NK cells in a dose-dependent manner (Figure 3c-d). The number of migrated NK cells was higher in ELK3-depleted than in control MDA-MB231 cells (Figure 3e-f). ELK3-depleted Hs578T cells also showed increased migration of NK cells (Figure 3g-i), suggesting that

cells. (h) Quantitative analysis of *ELK3* mRNA levels in Hs578T cells expressing shCon and shELK3#1. Error bars represent standard deviation; **** $p < 0.0001$ (unpaired two-tailed Student's t-test). (i) Quantitative analysis of *CXCL16* mRNA levels in Hs578T cells expressing shCon and shELK3#1. Error bars represent standard deviation; ** $p < 0.01$ (unpaired two-tailed Student's t-test). (j) Immunoblot analysis of ELK3 in Hs578T cells expressing shCon and shELK3#1. GAPDH was used as the loading control. (k) Immunoblot analysis of *CXCL16* in Hs578T cells expressing shCon and shELK3#1. GAPDH was used as the loading control. (l) Heatmap analysis of immune-related genes in Hs578T cells expressing shCon and shELK3#1.

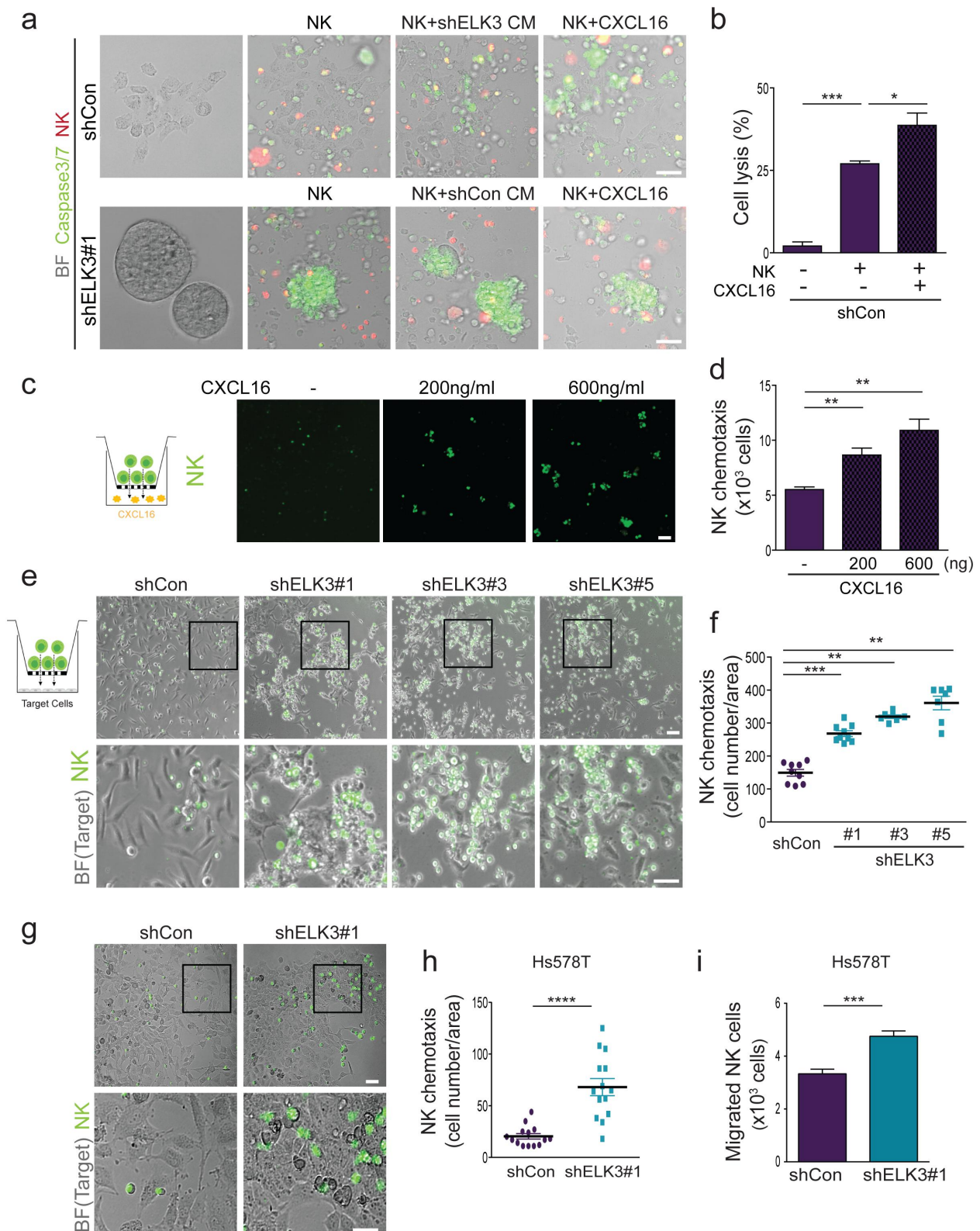


Figure 3. The chemotactic activity of CXCL16 recruits NK cells to target TNBC cells. (a) Immunofluorescence images of caspase 3/7 activity (green) in MDA-MB231 organoids expressing shCon and shELK3#1 after 4 h of coculture with FarRed-labeled NK92MI cells under the indicated conditions. The E:T ratio is 1:10. Scale bar, 100 μ m. (b) Rate of target cell death in MDA-MB231 cells expressing shCon after 4 h of coculture with CFSE-labeled NK92MI cells under the indicated conditions. The final concentration of CXCL16 protein was 200 ng/ml. The E:T ratio is 1:10. Error bars represent standard deviation; * p < 0.05, **** p < 0.001 (one-way ANOVA). (c) Immunofluorescence images of migrated NK92MI cells in response to recombinant CXCL16 protein. Scale bar, 200 μ m. (d) The graph indicates the number of migrated NK92MI cells in CXCL16-mediated chemotaxis. Error bars represent standard deviation; ** p < 0.01 (one-way ANOVA). (e) Migrated NK92MI cells in MDA-MB231 cells expressing shCon, shELK3#1, shELK3#3, and shELK3#5. Scale bar, 100 μ m, 200 μ m. (f) The graph indicates the number of migrated NK cells in MDA-MB231 cells expressing shCon, shELK3#1, shELK3#3, and shELK3#5. Error bars represent standard deviation; ** p < 0.01, *** p < 0.001 (one-way ANOVA). (g-i) Migrated NK92MI cells in Hs578T cells expressing shCon and shELK3#1. The graph indicates the number of migrated NK92MI cells in Hs578T cells expressing shCon and shELK3#1. Scale bar, 100 μ m, 200 μ m. Error bars represent standard deviation; ** p < 0.001, **** p < 0.0001 (unpaired two-tailed Student's t -test).

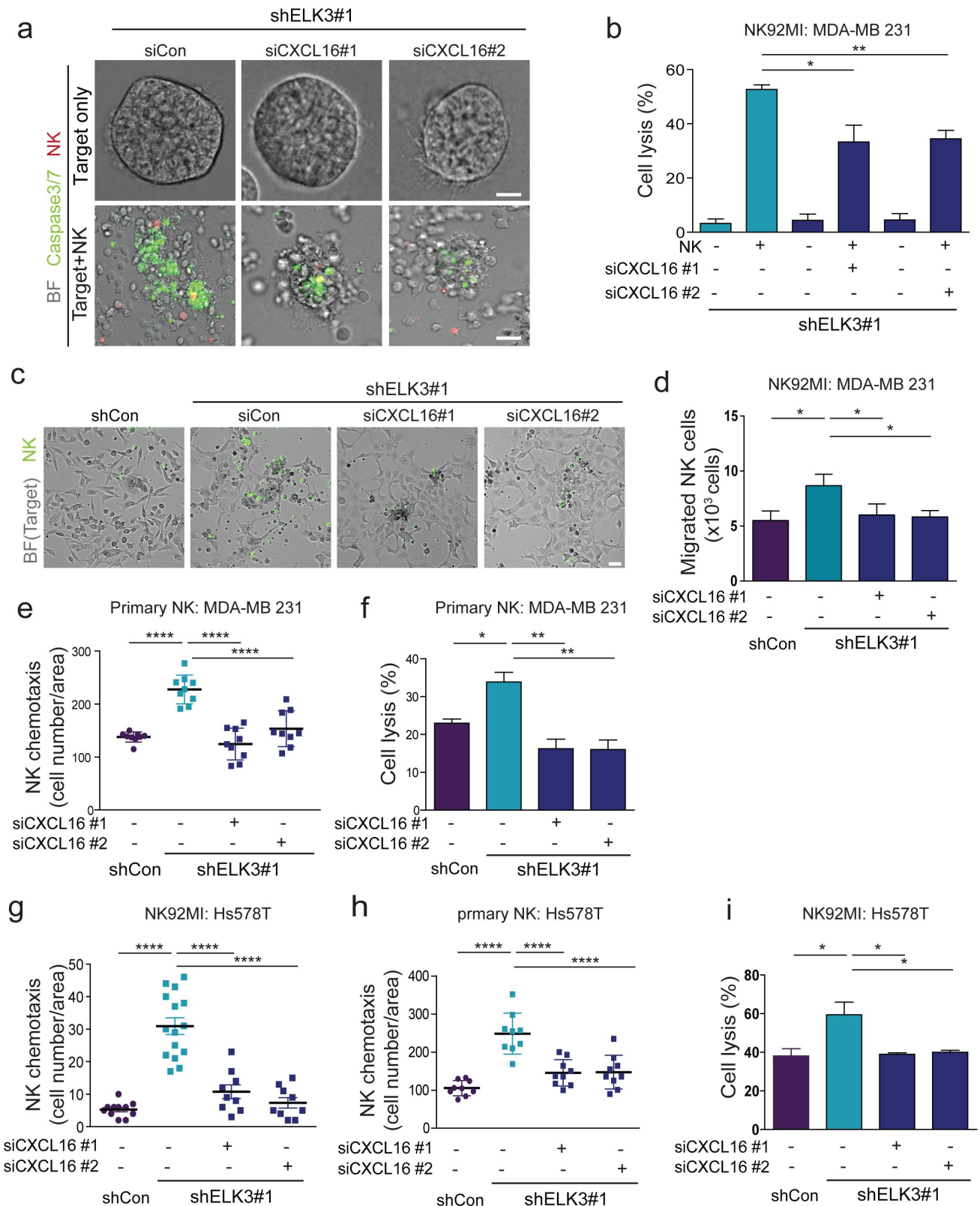


Figure 4. The ELK3-CXCL16 axis determines the response of NK cells in TNBC cells. (a) Immunofluorescence images of caspase 3/7 activity (green) in MDA-MB231 shELK3#1 organoids transfected with siCon, siCXCL16#1, and siCXCL16#2 after 4 h of coculture with FarRed-labeled NK92MI cells. The E:T ratio is 1:10. Scale bar, 50 μ m. (b) Rate of target cell death in MDA-MB231 shELK3#1 cells transfected with siCon siCXCL16#1, and siCXCL16#2 after 4 h of coculture with CFSE-labeled NK92MI cells. Error bars represent standard deviation; * p < 0.05, ** p < 0.01 (one-way ANOVA). (c) Migrated NK92MI cells in MDA-MB231 shELK3#1 cells transfected with siCon siCXCL16#1, and siCXCL16#2. Scale bar, 200 μ m. (d) The graph indicates the number of migrated NK92MI cells in MDA-MB231 shELK3#1 cells transfected with siCon siCXCL16#1, and siCXCL16#2. Error bars represent standard deviation; * p < 0.05 (one-way ANOVA). (e) Migrated primary NK cells in MDA-MB231 shELK3#1 cells transfected with siCon siCXCL16#1, and siCXCL16#2. Error bars represent standard deviation; **** p < 0.0001 (one-way ANOVA). (f) Rate of target cell death in MDA-MB231 shELK3#1 cells transfected with siCon siCXCL16#1, and siCXCL16#2 after 4 h of coculture with CFSE-labeled primary cells. Error bars represent standard deviation; * p < 0.05, ** p < 0.01 (one-way ANOVA). (g) Migrated NK92MI cells in Hs578T shELK3#1 cells transfected with siCon siCXCL16#1, and siCXCL16#2. Error bars represent standard deviation; **** p < 0.0001 (one-way ANOVA). (h) Migrated primary NK cells in Hs578T shELK3#1 cells transfected with siCon siCXCL16#1, and siCXCL16#2. Error bars represent standard deviation; **** p < 0.0001 (one-way ANOVA). (i) Rate of target cell death in Hs578T and Hs578T shELK3#1 cells transfected with siCon siCXCL16#1, and siCXCL16#2 after 4 h co-cultured with CFSE-labeled NK92MI cells. Error bars represent the standard deviation; * p < 0.05 (one-way ANOVA).

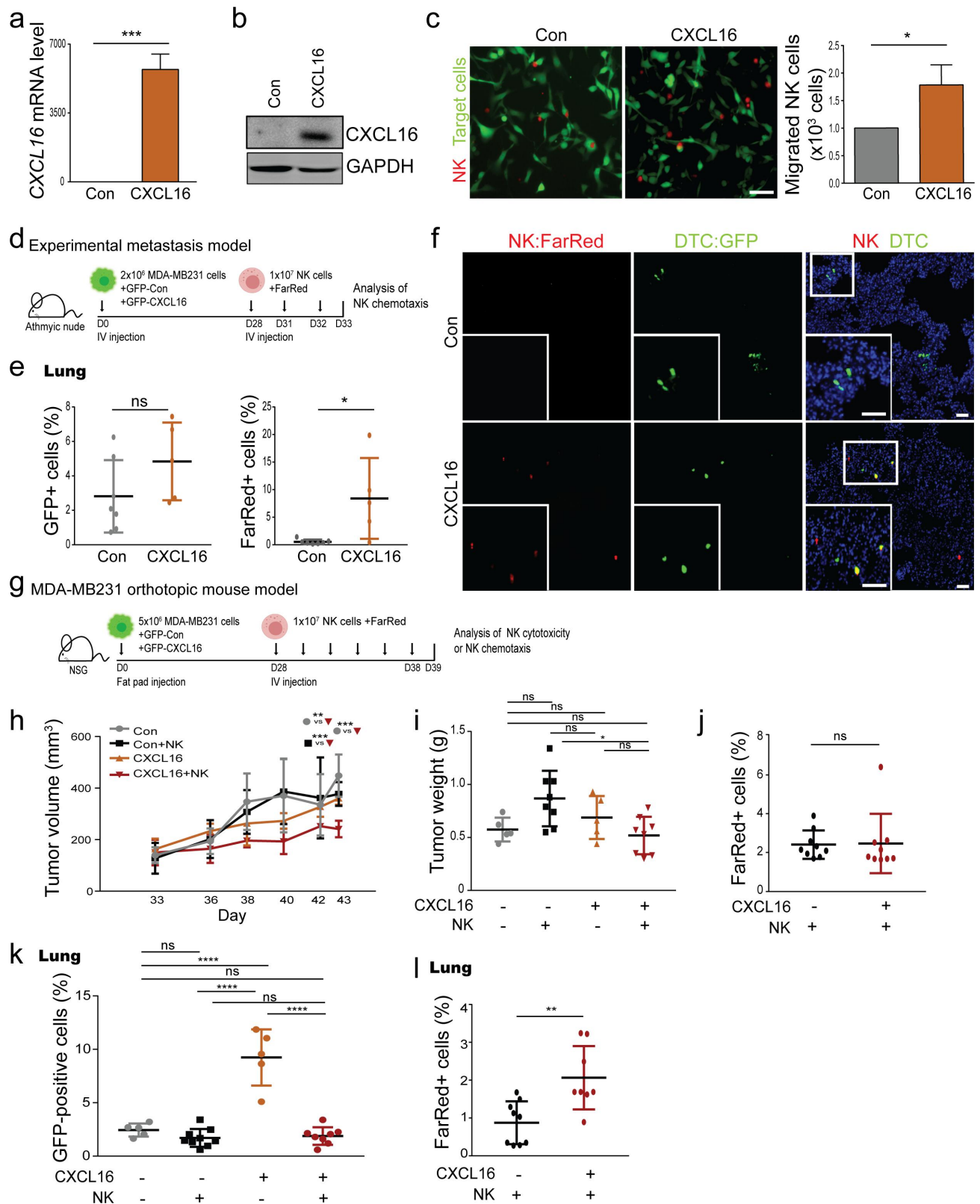


Figure 5. CXCL16 promotes NK cell chemotaxis and cytotoxicity *in vivo*. (a) Quantitative analysis of *CXCL16* mRNA levels in MDA-MB231-GFP-luciferase cells expressing control and CXCL16 (231-control and 231-CXCL16). Error bars represent standard deviation; *** $p < 0.001$ (unpaired two-tailed Student's *t*-test). (b) Immunoblot analysis of CXCL16 in 231-control and 231-CXCL16 cells. GAPDH was used as the loading control. (c) Migrated NK92MI cells in 231-control and 231-CXCL16 cells. Scale bar, 100 μ m. The graph indicates the number of migrated NK92MI cells in 231-control and 231-CXCL16 cells. Error bars represent standard deviation; * $p < 0.05$ (unpaired two-tailed Student's *t*-test). (d) Experimental scheme for NK cell recruitment in the experimental metastasis model. NK92MI cells were intravenously injected three times after 231-control and 231-CXCL16 cell injection. (e) The percentage of GFP-positive cells in the lungs from mice harboring 231-control and 231-CXCL16 cells after administration of NK92MI cells. GFP indicates tumor cells in the lung. FarRed indicates NK92MI cells in the lung. Error bars represent standard deviation; * $p < 0.05$ (unpaired two-tailed Student's *t*-test). NS is non-significant. (f) Immunofluorescence images of NK92MI cells in the lungs from mice harboring 231-control and 231-CXCL16 cells after NK92MI cell administration. Scale bar, 100 μ m, 200 μ m. (g) Experimental scheme for NK cell recruitment and NK cell cytotoxicity in the orthotopic mouse model. NK92MI cells were intravenously injected six times after visualization of primary tumors. (h) Primary tumor growth in mice harboring 231-control and 231-

CXCL16 promotes NK cell recruitment to tumor cells for NK cell-mediated cytotoxicity in TNBC

The ELK3-CXCL16 axis is essential for NK cell-mediated cytotoxicity

To further investigate whether a molecular link between ELK3 and CXCL16 is required for the immune response of NK cells, we used siRNA against the CXCL16 in ELK3-depleted MDA-MB231 and Hs578T cells. MDA-MB231 and Hs578T cells with siRNA against the CXCL16 gene significantly decreased CXCL16 mRNA and protein levels (Supplemental Figure 3a-d). CXCL16 depletion in ELK3-depleted MDA-MB231 cells suppressed NK cell-mediated apoptosis and cell death compared with control cells (Figure 4a-b). CXCL16 depletion remarkably suppressed the recruitment of NK cells to target cells in ELK3-depleted MDA-MB231 cells (Figure 4c-d). Indeed, primary NK cells consistently presented NK cell recruitment and cytotoxicity in the indicated conditions of MDA-MB231 cells (Figure 4e-f). In ELK3-depleted Hs578T cells, CXCL16 depletion inhibited NK cell cytotoxicity through NK cell recruitment (Figure 4g-i). These data suggest that ELK3 depletion-mediated CXCL16 induction contributes to increasing the immune response in TNBC.

CXCL16 promotes the infiltration of NK cells to control cancer progression in vivo

To determine whether CXCL16 recruited NK cells to tumors in TNBC mouse model, we generated MDA-MB231 cells overexpressing GFP (231-control) and overexpressing GFP and CXCL16 (231-CXCL16) (Figure 5a-b). *In vitro* transwell assays showed that the number of migrated NK cells was higher in 231-CXCL16 cells than in 231-control cells (Figure 5c). To further investigate whether CXCL16 induced the infiltration of NK cells in the TNBC mouse model, we evaluated the recruitment of NK cells using an experimental metastasis mouse model. 231-control and 231-CXCL16 cells were intravenously injected into mice for 28 days to change the microenvironment to one that favors immune cells, followed by intravenous injection of FarRed-labeled NK cells (Figure 5d). After 33 days, harvested lung tissues were dissociated, and the number of NK cells was estimated by flow cytometry. Lungs from mice harboring 231-CXCL16 cells had a higher number of NK (FarRed) cells than those from control mice (Figure 5e). NK cells were nearly localized to disseminated tumor cells (DTCs) overexpressing CXCL16 in the lung (Figure 5f), suggesting that CXCL16 altered the TME to attract NK cell recruitment. Next, we examined whether the function of CXCL16 in the regulation of primary

cancer and metastatic growth in TNBC orthotopic mouse model. 231-control and 231-CXCL16 cells were injected into the mammary glands of mice for 28 days, followed by intravenous injection of FarRed-labeled NK cells (Figure 5g). Mice harboring 231-CXCL16 cells showed a statistically significant suppressive tumor growth compared with mice harboring 231-control cells, suggesting an anticancer effect of NK cells (Figure 5h-i). However, the number of NK cells in the tumor did not differ between the control and CXCL16 groups because of the rare population of NK cells (Figure 5j). NK cell administration significantly inhibited the dissemination of tumor cells into the lung by increasing NK cell recruitment in mice harboring 231-CXCL16 cells (Figure 5k-l). These data suggest that CXCL16 promotes the infiltration of NK cells to suppress primary tumor and metastatic growth in the TNBC mouse model.

ELK3 and CXCL16 are negatively correlated in human breast cancer patients

To determine whether the molecular relationship between ELK3 and CXCL16 controls breast cancer progression, we performed *in silico* analysis using TCGA database. The results of *in silico* analysis showed a negative correlation between ELK3 and CXCL16 mRNA levels in human breast cancer patient samples but not in TNBC samples (Figure 6a). The survival rate was slightly higher in patients with low expression of ELK3 and high expression of CXCL16 (Figure 6b). Large scale survival analysis showed that low expression of ELK3 and high expression of CXCL16 were significantly associated with good prognosis of human breast cancer patients (Figure 6c). To determine whether the molecular link between ELK3 and CXCL16 predicts NK cell recruitment in human breast cancer patients, we analyzed NK cell gene signatures in breast cancer patient samples. For this purpose, NK cell-related genes were used as described in a previous report.³⁹ Low expression of CXCL16 was associated with low expression of NK cell-related genes, which indicates a low number of NK cells in the patient samples (Figure 6d_white box). Samples showing low expression of ELK3 and high expression of CXCL16 had increased expression of NK cell-regulated genes (Figure 6d_yellow box and 6e), indicating that CXCL16 may promote NK cell recruitment, thereby inducing the formation of an immune-sensitive TME. These data suggest that ELK3 could be a promising candidate target to increase the efficacy of NK cell therapy in breast cancer.

Discussion

In this study, we demonstrated that CXCL16 is increased by ELK3 depletion and promotes the recruitment of NK cells to

CXCL16 cells after NK92MI cell administration. Error bars represent standard deviation; **p < 0.01, ***p < 0.001 (two-way ANOVA, multiple comparisons). The gray circle indicates the control group. The black box indicates the control with NK92MI administration group. The red triangle indicates the CXCL16 with NK92MI administration group. (i) The analysis of primary tumor weight from mice harboring 231-control and 231-CXCL16 cells after NK92MI cell administration. Error bars represent standard deviation; *p < 0.05 (one-way ANOVA, multiple comparisons). NS is non-significant. (j) The percentage of FarRed-positive cells in the primary tumor from the mouse harboring 231-control and 231-CXCL16 cells after indicated NK92MI cells administration. FarRed indicates NK92MI cells in the tumor. Error bars represent the standard deviation. NS is non-significant. Error bars represent the standard deviation; *p < 0.05 (Unpaired two-tailed Student's t-test). (k-l) The percentage of GFP and FarRed-positive cells in the lung from the mouse harboring 231-control and 231-CXCL16 cells after indicated NK92MI cells administration. GFP indicates disseminated tumor cells in the lung. FarRed indicates NK92MI cells in the lung. Error bars represent standard deviation; **p < 0.01 (one-way ANOVA, multiple comparisons, unpaired two-tailed Student's t-test).

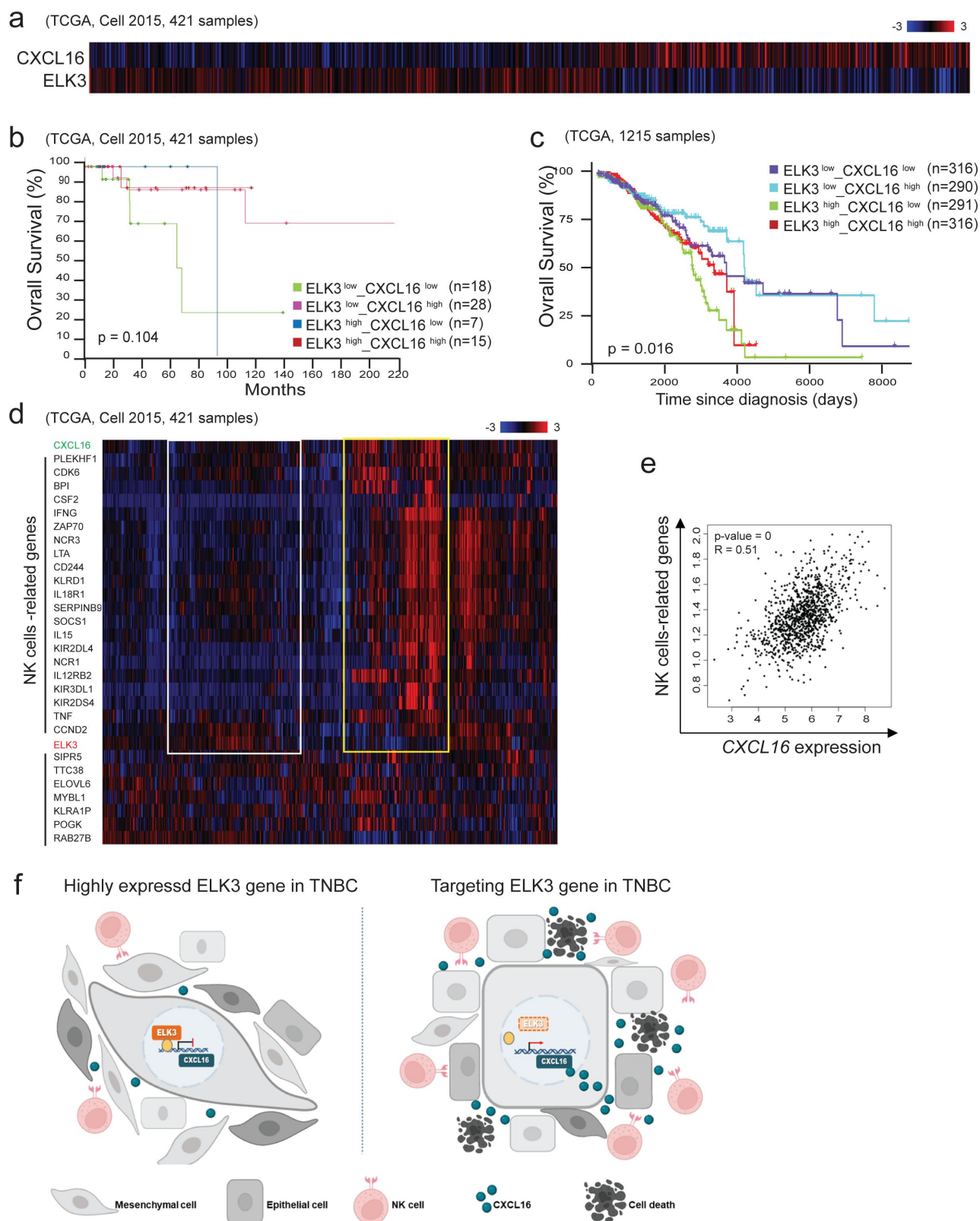


Figure 6. Negative correlation between ELK3 and CXCL16 in human breast cancer. (a) Expression analysis of *ELK3* and *CXCL16* in 421 human breast cancer patient samples (TCGA database). (b-c) Kaplan–Meier survival plots showing the overall survival of breast cancer patients. (d) Heatmap analysis of *ELK3*, *CXCL16*, and NK cell-related genes³⁷ in 421 human breast cancer patient samples. The white box indicates the patient samples with high expression of the *ELK3* gene and low expression of the *CXCL16* gene. The yellow box indicates patient samples with low expression of the *ELK3* gene and high expression of the *CXCL16* gene. (e) Correlation analysis of *CXCL16* and NK cell-related genes in human breast cancer patient samples. (f) The biological role of ELK3–CXCL16 axis on NK cell cytotoxicity. ELK3 depletion increased secreted CXCL16 protein to recruit NK cells and resulted in improved NK cell cytotoxicity in TNBC cells.

boost NK cell cytotoxicity *in vitro* and *in vivo* (Figure 6f). *In silico* analysis showed that high expression of ELK3 is associated with low expression of CXCL16 in various breast cancer cell lines and human breast cancer patient samples. Breast cancer patients harboring low expression of ELK3 and high expression of CXCL16 had a better survival rate than others. These findings suggest that targeting *ELK3* could improve NK cell therapy by promoting the recruitment of immune cells in TNBC.

Chemokines play an important role in regulating the migration of immune cells to the TME as promoters and suppressors of tumor progression via immune cell recruitment.^{44–46} The role of immune cell infiltration induced by chemokines in tumor regression remains controversial. CXCR3 and CXCR4 ligands induce the infiltration of NK cells and T cells into tumors.^{47–49} In addition, studies suggest that radiation-induced CXCL16 acts as a chemokine to attract NK cells and T cells in breast cancer.^{50,51} In line with previous results, the present findings demonstrated that CXCL16-induced NK92MI and primary NK cell recruitment suppressed breast cancer progression in an *in vivo* system.

The results of this study indicate that ELK3 represses CXCL16 expression to confer immune-evasive properties in the MDA-MB231 and Hs578T cell lines. Considering that TNBC with high ELK3 expression has low reactivity to NK cells, and that ELK3 suppression renders cancer cells susceptible to NK cells, ELK3 may regulate the immune response in breast cancer, including TNBCs with high expression of the *ELK3* gene. However, the role of the ELK3-CXCL16 axis in the NK cell response was only examined in human TNBC in this study. Future studies should examine the function of this molecular axis in immune systems using syngeneic mouse TNBC models to gain a better understanding of the role of ELK3 in innate and adaptive immunity, and ultimately contribute to improving the effect of immune therapies.

ELK3 transcriptionally regulates cell migration-related genes in various cancer types including breast cancer.^{25,28,29,52} In addition, ELK3 controls immune response-related genes including chemokines to modulate the immune response.³² Combined with the role of CXCL16 in the response to NK92MI and primary NK cells, ELK3 might play a pleiotropic role in regulating multiple genes involved in different biological processes, including cancer progression and immune responses. In this study, we suggested that ELK3 indirectly regulated CXCL16 expression levels because ELK3 was not binding on the promoter of *CXCL16* gene. Further investigation of the molecular link between ELK3 and CXCL16 will expand our understanding of ELK3-mediated immune responses in TNBC, which may support the efficacy of targeting *ELK3* for improving immune therapeutic effects.

Acknowledgments

We specially thank Seung Hee Choi and Issac Kim for primary NK purification and expansion of human PBMC. We thank Young-ho Ahn (Ewha Womans University) for kindly providing pLVX DNA constructs.

H-YJ, DL, SHC, JDP, and E-SK: experimental performance, data acquisition, and data analysis. H-YJ, ML, and JL: *in silico* analysis with microarray and TCGA data. H-YJ and K-SP: experimental design and data interpretation. H-YJ and K-SP: writing of the manuscript.

Disclosure statement

No potential conflict of interest was reported by the authors.

Funding

This research was supported by Basic Science Research Program through the National Research Foundation of Korea (NRF) funded by the Ministry of Education (No. NRF-2019R1A6A1A03032888 and NRF-2022R1A2C1003390; to K-S Park). This work was also supported by the NRF (NRF-2019R1I1A1A01060649 and 2022R1I1A1A01070767; to H-Y Jung) and supported by the Ministry of Science and ICT and the Korea Institute of Radiological and Medical Sciences (50531-2023; to H-Y Jung).

Data availability statement

The data are available in a public, open access repository. All data relevant to the study are included in the article or uploaded as supplementary information.

Ethics approval

All participants provided written informed consents authorizing the collection and use of their blood for study purposes. This study was approved by institutional review board (IRB) of CHA University (1044308-202112-HR-097-02).

References

1. Mayor M, Yang N, Sterman D, Jones DR, Adusumilli PS. Immunotherapy for non-small cell lung cancer: current concepts and clinical trials. *Eur J Cardiothorac Surg.* 2016;49(5):1324–1333. doi:10.1093/ejcts/ezv371.
2. Luke JJ, Flaherty KT, Ribas A, Long GV. Targeted agents and immunotherapies: optimizing outcomes in melanoma. *Nat Rev Clin Oncol.* 2017;14(8):463–482. doi:10.1038/nrclinonc.2017.43.
3. Rosenberg SA, Packard BS, Aebersold PM, Solomon D, Topalian SL, Toy ST, Simon P, Lotze MT, Yang JC, Seipp CA, et al. Use of tumor-infiltrating lymphocytes and interleukin-2 in the immunotherapy of patients with metastatic melanoma. A preliminary report. *N Engl J Med.* 1988;319(25):1676–1680. doi:10.1056/NEJM19881223192527.
4. Rosenberg SA, Yang JC, Sherry RM, Kammula US, Hughes MS, Phan GQ, Citrin DE, Restifo NP, Robbins PF, Wunderlich JR, et al. Durable complete responses in heavily pretreated patients with metastatic melanoma using T-cell transfer immunotherapy. *Clin Cancer Res.* 2011;17(13):4550–4557. doi:10.1158/1078-0432.CCR-11-0116.
5. Zacharakis N, Chinnasamy H, Black M, Xu H, Lu YC, Zheng Z, Pasetto A, Langhan M, Shelton T, Prickett T, et al. Immune recognition of somatic mutations leading to complete durable regression in metastatic breast cancer. *Nat Med.* 2018;24(6):724–730. doi:10.1038/s41591-018-0040-8.
6. Esfahani K, Roudaia L, Buhlaiga N, Del Rincon SV, Papneja N, Miller WH Jr. A review of cancer immunotherapy: from the past, to the present, to the future. *Curr Oncol.* 2020;27(Suppl 2):S87–97. doi:10.3747/co.27.5223.
7. O'donnell JS, Teng MWL, Smyth MJ. Cancer immunoeediting and resistance to T cell-based immunotherapy. *Nat Rev Clin Oncol.* 2019;16(3):151–167. doi:10.1038/s41571-018-0142-8.
8. Rohaan MW, Wilgenhof S, Haanen J. Adoptive cellular therapies: the current landscape. *Virchows Arch.* 2019;474(4):449–461. doi:10.1007/s00428-018-2484-0.
9. Vivier E, Tomasello E, Baratin M, Walzer T, Ugolini S. Functions of natural killer cells. *Nat Immunol.* 2008;9(5):503–510. doi:10.1038/ni1582.

10. Torres Cepeda TE, Alanis Guzman MG, Maiti R. Relationship between nutritional composition and anatomical parameters in sorghum (*Sorghum bicolor* L. Moench). *Arch Latinoam Nutr.* 1996;46:253–259.
11. Imai K, Matsuyama S, Miyake S, Suga K, Nakachi K. Natural cytotoxic activity of peripheral-blood lymphocytes and cancer incidence: an 11-year follow-up study of a general population. *Lancet.* 2000;356(9244):1795–1799. doi:10.1016/S0140-6736(00)03231-1.
12. Shimasaki N, Jain A, Campana D. NK cells for cancer immunotherapy. *Nat Rev Drug Discov.* 2020;19(3):200–218. doi:10.1038/s41573-019-0052-1.
13. Lopez-Soto A, Gonzalez S, Smyth MJ, Galluzzi L. Control of Metastasis by NK Cells. *Cancer Cell.* 2017;32(2):135–154. doi:10.1016/j.ccell.2017.06.009.
14. Bald T, Krummel MF, Smyth MJ, Barry KC. The NK cell-cancer cycle: advances and new challenges in NK cell-based immunotherapies. *Nat Immunol.* 2020;21(8):835–847. doi:10.1038/s41590-020-0728-z.
15. Li Y, Yin J, Li T, Huang S, Yan H, Leavenworth J, Wang X. NK cell-based cancer immunotherapy: from basic biology to clinical application. *Sci China Life Sci.* 2015;58(12):1233–1245. doi:10.1007/s11427-015-4970-9.
16. Melaiu O, Lucarini V, Cifaldi L, Fruci D. Influence of the Tumor Microenvironment on NK cell function in solid Tumors. *Front Immunol.* 2019;10:3038. doi:10.3389/fimmu.2019.03038.
17. Habif G, Crinier A, Andre P, Vivier E, Narni-Mancinelli E. Targeting natural killer cells in solid tumors. *Cell Mol Immunol.* 2019;16(5):415–422. doi:10.1038/s41423-019-0224-2.
18. Cozar B, Greppi M, Carpentier S, Narni-Mancinelli E, Chiosso L, Vivier E. Tumor-infiltrating natural killer cells. *Cancer Discov.* 2021;11(1):34–44. doi:10.1158/2159-8290.CD-20-0655.
19. Ali TH, Pisanti S, Ciaglia E, Mortarini R, Anichini A, Garofalo C, Talerico R, Santinami M, Gulletta E, Ietto C, et al. Enrichment of CD56(dim)KIR + CD57 + highly cytotoxic NK cells in tumour-infiltrated lymph nodes of melanoma patients. *Nat Commun.* 2014;5(1):5639. doi:10.1038/ncomms6639.
20. Rusakiewicz S, Semeraro M, Sarabi M, Desbois M, Locher C, Mendez R, Vimond N, Concha A, Garrido F, Isambert N, et al. Immune infiltrates are prognostic factors in localized gastrointestinal stromal tumors. *Cancer Res.* 2013;73(12):3499–3510. doi:10.1158/0008-5472.CAN-13-0371.
21. Chow MT, Luster AD. Chemokines in cancer. *Cancer Immunol Res.* 2014;2(12):1125–1131. doi:10.1158/2326-6066.CIR-14-0160.
22. Bule P, Aguiar SI, Aires-Da-Silva F, Dias JNR. Chemokine-directed Tumor microenvironment Modulation in Cancer Immunotherapy. *Int J Mol Sci.* 2021;22(18):9804. doi:10.3390/ijms22189804.
23. Zhao Q, Ren Y, Xie H, Yu L, Lu J, Jiang W, Xiao W, Zhu Z, Wan R, Li B. ELK3 mediated by ZEB1 facilitates the growth and metastasis of Pancreatic carcinoma by activating the Wnt/ β -catenin pathway. *Front Cell Dev Biol.* 2021;9:700192. doi:10.3389/fcell.2021.700192.
24. Liu Z, Ren Z, Zhang C, Qian R, Wang H, Wang J, Zhang W, Liu B, Lian X, Wang Y, et al. ELK3: a new molecular marker for the diagnosis and Prognosis of Glioma. *Front Oncol.* 2021;11:608748. doi:10.3389/fonc.2021.608748.
25. Kim KS, Park JI, Oh N, Cho HJ, Park JH, Park KS. ELK3 expressed in lymphatic endothelial cells promotes breast cancer progression and metastasis through exosomal miRNAs. *Sci Rep.* 2019;9(1):8418. doi:10.1038/s41598-019-44828-6.
26. Cho HJ, Oh N, Park JH, Kim KS, Kim HK, Lee E, Hwang S, Kim S-J, Park K-S. ZEB1 Collaborates with ELK3 to repress E-Cadherin expression in Triple-negative breast cancer cells. *Mol Cancer Res.* 2019;17(11):2257–2266. doi:10.1158/1541-7786.MCR-19-0380.
27. Park JD, Kim KS, Choi SH, Jo GH, Choi JH, Park SW, Ko E-S, Lee M, Lee D-K, Jang HJ, et al. ELK3 modulates the antitumor efficacy of natural killer cells against triple negative breast cancer by regulating mitochondrial dynamics. *J ImmunoTher Cancer.* 2022;10(7):e004825. doi:10.1136/jitc-2022-004825.
28. Kim HK, Park JD, Choi SH, Shin DJ, Hwang S, Jung HY, Park K-S. Functional link between miR-200a and ELK3 regulates the metastatic nature of breast cancer. *Cancers (Basel).* 2020;12(5):1225. doi:10.3390/cancers12051225.
29. Lee M, Cho HJ, Park KS, Jung HY. ELK3 controls Gastric cancer cell migration and invasion by regulating ECM remodeling-related genes. *Int J Mol Sci.* 2022;23(7):3709. doi:10.3390/ijms23073709.
30. Oh N, Park JI, Park JH, Kim KS, Lee DR, Park KS. The role of ELK3 to regulate peritumoral lymphangiogenesis and VEGF-C production in triple negative breast cancer cells. *Biochem Biophys Res Commun.* 2017;484(4):896–902. doi:10.1016/j.bbrc.2017.02.030.
31. Zhuo W, Jia L, Song N, Lu XA, Ding Y, Wang X, Song X, Fu Y, Luo Y. The CXCL12–CXCR4 Chemokine Pathway: a novel axis regulates Lymphangiogenesis. *Clin Cancer Res.* 2012;18(19):5387–5398. doi:10.1158/1078-0432.CCR-12-0708.
32. Tsoyi K, Geldart AM, Christou H, Liu X, Chung SW, Perrella MA. Elk-3 is a KLF4-regulated gene that modulates the phagocytosis of bacteria by macrophages. *J Leukoc Biol.* 2015;97(1):171–180. doi:10.1189/jlb.4A0214-087R.
33. Dazhi W, Zheng J, Chunling R. High ELK3 expression is associated with the VEGF-C/VEGFR-3 axis and gastric tumorigenesis and enhances infiltration of M2 macrophages. *Future Med Chem.* 2020;12(24):2209–2224. doi:10.4155/fmc-2019-0337.
34. Choi YH, Lim EJ, Kim SW, Moon YW, Park KS, An HJ. IL-27 enhances IL-15/IL-18-mediated activation of human natural killer cells. *J ImmunoTher Cancer.* 2019;7(1):168. doi:10.1186/s40425-019-0652-7.
35. Livak KJ, Schmittgen TD. Analysis of relative gene expression data using real-time quantitative PCR and the 2^{-Delta Delta} C(T) Method. *Methods.* 2001;25(4):402–408. doi:10.1006/meth.2001.1262.
36. Jung HY, Fattet L, Tsai JH, Kajimoto T, Chang Q, Newton AC, Yang J. Apical–basal polarity inhibits epithelial–mesenchymal transition and tumour metastasis by PAR-complex-mediated SNAI1 degradation. *Nat Cell Biol.* 2019;21(3):359–371. doi:10.1038/s41556-019-0291-8.
37. Kong SY, Kim KS, Kim J, Kim MK, Lee KH, Lee JY, Oh N, Park J-I, Park J-H, Heo S-H, et al. The ELK3–GATA3 axis orchestrates invasion and metastasis of breast cancer cells in vitro and in vivo. *Oncotarget.* 2016;7(40):65137–65146. doi:10.18632/oncotarget.11427.
38. Colaprico A, Silva TC, Olsen C, Garofano L, Cava C, Garolini D, Sabedot TS, Malta TM, Pagnotta SM, Castiglioni I, et al. Tcgbiolinks: an R/Bioconductor package for integrative analysis of TCGA data. *Nucleic Acids Res.* 2016;44(8):e71. doi:10.1093/nar/gkv1507.
39. Cursons J, Souza-Fonseca-Guimaraes F, Foroutan M, Anderson A, Hollande F, Hediye-Zadeh S, Behren A, Huntington ND, Davis MJ. A Gene signature predicting natural killer cell infiltration and improved Survival in Melanoma patients. *Cancer Immunol Res.* 2019;7(7):1162–1174. doi:10.1158/2326-6066.CIR-18-0500.
40. Grundemann C, Bauer M, Schweier O, von Oppen N, Lassing U, Saudan P, Becker K-F, Karp K, Hanke T, Bachmann MF, et al. Cutting edge: identification of E-cadherin as a ligand for the murine killer cell lectin-like receptor G1. *J Immunol.* 2006;176(3):1311–1315. doi:10.4049/jimmunol.176.3.1311.
41. Chockley PJ, Chen J, Chen G, Beer DG, Standiford TJ, Keshamouni VG. Epithelial-mesenchymal transition leads to NK cell-mediated metastasis-specific immunosurveillance in lung cancer. *J Clin Invest.* 2018;128(4):1384–1396. doi:10.1172/JCI97611.
42. Fauriat C, Long EO, Ljunggren HG, Bryceson YT. Regulation of human NK-cell cytokine and chemokine production by target cell recognition. *Blood.* 2010;115(11):2167–2176. doi:10.1182/blood-2009-08-238469.

43. Maghazachi AA. Role of chemokines in the biology of natural killer cells. *Curr Top Microbiol Immunol.* **2010**;341:37–58.
44. Kohli K, Pillarisetty VG, Kim TS. Key chemokines direct migration of immune cells in solid tumors. *Cancer Gene Ther.* **2022**;29(1):10–21. doi:10.1038/s41417-021-00303-x.
45. Burugu S, Asleh-Aburaya K, Nielsen TO. Immune infiltrates in the breast cancer microenvironment: detection, characterization and clinical implication. *Breast Cancer.* **2017**;24(1):3–15. doi:10.1007/s12282-016-0698-z.
46. Guillerey C, Huntington ND, Smyth MJ. Targeting natural killer cells in cancer immunotherapy. *Nat Immunol.* **2016**;17(9):1025–1036. doi:10.1038/ni.3518.
47. Wendel M, Galani IE, Suri-Payer E, Cerwenka A. Natural killer cell accumulation in tumors is dependent on IFN-gamma and CXCR3 ligands. *Cancer Res.* **2008**;68(20):8437–8445. doi:10.1158/0008-5472.CAN-08-1440.
48. Mikucki ME, Fisher DT, Matsuzaki J, Skitzki JJ, Gaulin NB, Muhitch JB, Ku AW, Frelinger JG, Odunsi K, Gajewski TF, et al. Non-redundant requirement for CXCR3 signalling during tumoricidal T-cell trafficking across tumour vascular checkpoints. *Nat Commun.* **2015**;6(1):7458. doi:10.1038/ncomms8458.
49. Seo YD, Jiang X, Sullivan KM, Jalikis FG, Smythe KS, Abbasi A, Vignali M, Park JO, Daniel SK, Pollack SM, et al. Mobilization of CD8(+) T cells via CXCR4 Blockade Facilitates PD-1 Checkpoint therapy in human Pancreatic cancer. *Clin Cancer Res.* **2019**;25(13):3934–3945. doi:10.1158/1078-0432.CCR-19-0081.
50. Matsumura S, Wang B, Kawashima N, Braunstein S, Badura M, Cameron TO, Babb JS, Schneider RJ, Formenti SC, Dustin ML, et al. Radiation-induced CXCL16 release by breast cancer cells attracts effector T cells. *J Immunol.* **2008**;181(5):3099–3107. doi:10.4049/jimmunol.181.5.3099.
51. Yoon MS, Pham CT, Phan MT, Shin DJ, Jang YY, Park MH, Kim S-K, Kim S, Cho D. Irradiation of breast cancer cells enhances CXCL16 ligand expression and induces the migration of natural killer cells expressing the CXCR6 receptor. *Cytotherapy.* **2016**;18(12):1532–1542. doi:10.1016/j.jcyt.2016.08.006.
52. Yang H, Schramek D, Adam R C, Keyes B E, Wang P, Zheng D, Fuchs E. ETS family transcriptional regulators drive chromatin dynamics and malignancy in squamous cell carcinomas. *Elife.* **2015**;4:e10870. doi:10.7554/eLife.10870.